



**HAL**  
open science

## Use of alkali activated high-calcium fly ash binder for kaolin clay soil stabilisation: Physicochemical evolution

Elodie Coudert, Michael Paris, Dimitri Deneele, Giacomo Russo, Alessandro Tarantino

### ► To cite this version:

Elodie Coudert, Michael Paris, Dimitri Deneele, Giacomo Russo, Alessandro Tarantino. Use of alkali activated high-calcium fly ash binder for kaolin clay soil stabilisation: Physicochemical evolution. *Construction and Building Materials*, 2019, 201, 14p. 10.1016/j.conbuildmat.2018.12.188 . hal-01976909

**HAL Id: hal-01976909**

**<https://hal.science/hal-01976909v1>**

Submitted on 21 Oct 2021

**HAL** is a multi-disciplinary open access archive for the deposit and dissemination of scientific research documents, whether they are published or not. The documents may come from teaching and research institutions in France or abroad, or from public or private research centers.

L'archive ouverte pluridisciplinaire **HAL**, est destinée au dépôt et à la diffusion de documents scientifiques de niveau recherche, publiés ou non, émanant des établissements d'enseignement et de recherche français ou étrangers, des laboratoires publics ou privés.



Distributed under a Creative Commons Attribution - NonCommercial 4.0 International License

1 **Use of alkali activated high-calcium fly ash binder for kaolin clay soil stabilisation:**

2 **Physicochemical evolution**

3

4 Elodie Coudert<sup>a,b,c</sup>, Michael Paris<sup>a</sup>, Dimitri Deneele<sup>a,d\*</sup>, Giacomo Russo<sup>b</sup>, Alessandro  
5 Tarantino<sup>c</sup>

6 <sup>a</sup> Institut des Matériaux Jean Rouxel (IMN), Université de Nantes, CNRS, 2 rue de la  
7 Houssinière, BP 32229, 44322 Nantes Cedex 3, France

8 <sup>b</sup> Department of Civil and Mechanical Engineering, University of Cassino and Southern  
9 Lazio, Via Gaetano di Biasio, 43, 03043 Cassino, FR, Italy

10 <sup>c</sup> Department of Civil and Environmental Engineering, University of Strathclyde, 75  
11 Montrose Street, Glasgow, Scotland, G1 1XJ, United Kingdom

12 <sup>d</sup> IFSTTAR, GERS, EE, F-44344 Bouguenais, France.

13 \*Corresponding author

14 Phone : + 33 2 40 84 58 02

15 Fax: + 33 2 40 58 57 77

16 E-mail: Dimitri.Deneele@ifsttar.fr

17 **Abstract**

18 This study addresses the use of alkali activated high-calcium fly ash-based binder to  
19 improve engineering characteristics of soft clay-rich soils as an alternative to common  
20 stabilisers. The physico-chemical reaction sequence has been investigated by  
21 considering the binder alone and the binder mixed with kaolin. An insight into the  
22 reactivity evidenced that calcium-containing phases derived from high-calcium fly ash  
23 represent the reactive phases and, hence, pozzolanic activity is the dominant process.  
24 New compounds are formed, thenardite  $\text{Na}_2\text{SO}_4$  and an amorphous silicate consisting of

25 chains combined with calcium probably incorporating three-dimensional four-fold  
26 aluminium environments.

27 **Keywords**

28 Soil stabilisation; Alkali activated material; Kaolin; High-calcium fly ash

29

30 **1. Introduction**

31 Soft clay-rich soils are frequently encountered in construction sites. Their poor  
32 mechanical performance represents a critical issue in engineering projects. These soils  
33 cannot be directly used as earthfill materials and may cause excessive settlements of  
34 foundation structures. To improve their engineering characteristics chemical  
35 stabilisation involving the addition of a binder to the soil has been widely practiced. The  
36 commonly used stabilisers are Ordinary Portland Cement and lime whose stabilisation  
37 mechanisms have been widely reported [1-7]. Nevertheless, a major issue with those  
38 conventional stabilisers is a very significant environmental penalty due to high carbon  
39 dioxide emissions and energy intensive processes.

40 In the low carbon agenda, the development of novel technologies that are both cost- and  
41 carbon-efficient is of prime importance, particularly in the construction sector for which  
42 cement production contributes to at least 5–8% of global carbon dioxide emissions [8].  
43 As an alternative, industrial by-products such as high-calcium fly ash, rice husk ash, and  
44 silica fume have been successfully mixed as cementing additives to soft soils resulting  
45 in environmental and economic benefits [9-15].

46 Another alternative gaining attention is the use of Alkali Activated Materials as a viable  
47 sustainable binder whose often-claimed advantage is a much lower CO<sub>2</sub> emission  
48 process compared to traditional Portland cement. Works on alkali activated soils are  
49 recent and aim to stabilise different types of soil from clayey soil [16-17], sandy clay  
50 [18], Lateritic soils [19] marl, marlstone [20], silty sand [21], road aggregates [22] to  
51 mixed soil synthesised in laboratory [23-24]. The overall work shows the potential of  
52 alkaline activation for soil improvement, and this for different designed applications i.e.  
53 in deep soft soil [18], at shallow depth [24] or in rammed earth construction [25].

54 Alkali Activated Materials are defined as any binder system derived by the reaction of  
55 an alkali metal source (usually alkali hydroxide and alkali silicate solutions) with a solid  
56 aluminosilicate powder (commonly metakaolin, fly ash, blast furnace slag or natural  
57 pozzolan) [26-27]. It gives a hardened material at room temperature with mechanical  
58 properties potentially suitable for Portland cement replacement.

59 The type of aluminosilicate material needed in the alkali activation process varies as  
60 well. In fact, most of the studies were conducted on the use of fly ash [16-18; 20-21;23-  
61 25; 28-29]. Nevertheless, Zhang et al. [24] also examined the feasibility of metakaolin  
62 based alkali activated soil, and some other studies established on slag based alkali  
63 activated soil are as well existing [16, 17, 23].

64 As stabilisation using alkaline activation is a recent research area, studies about the  
65 understanding of the physicochemical reactivity of such systems have received little  
66 attention so far [17] . Yet, the molecular structure and the chemical composition of the  
67 alkali activated binders is essential to properly assess the resulting strength and  
68 durability of the final material.

69 This work focuses on the use of calcium-rich high-calcium fly ash from coal  
70 combustion activated by sodium-based alkaline solution as a binder for clay kaolin  
71 stabilisation. High-calcium fly ash was selected in the context of resource-saving being  
72 an industrial waste. Kaolin was selected as a model soil to represent a wide class of  
73 clays encountered in engineering projects.

74 The study was designed in three stages. An initial stage consisted in the investigation of  
75 the reactivity of the alkali activated high-calcium fly ash binder by itself, including (i)  
76 which phases are present and which phases are accessible during alkaline activation, (ii)  
77 which compounds are subsequently formed, and (iii) reactivity timescale. A second

78 stage focused on the interaction of the high-calcium fly ash-based binder with the kaolin  
79 clay to understand how the presence of kaolin modifies the reactivity of the system.  
80 Kaolinite is generally unreactive to alkali attack at ambient temperature. However, the  
81 addition of clay may affect chemical reactions as occurs in clay-cement mix [30].  
82 Finally, the physicochemical evolution occurring in the alkali activated high-calcium fly  
83 ash is compared with one occurring in the same kaolin stabilised by i) lime or ii) a mix  
84 of lime and the same high-calcium fly ash used in this experimental programme. This is  
85 aimed at assessing the potential benefit of high-calcium fly ash-based binder compared  
86 to the more traditional lime.  
87

88 **2. Material and methods**

89 *2.1 Materials*

90 A Polish high-calcium fly ash derived from hard coal and coal slime combustion in  
91 fluidised bed boiler was used. Its chemical analysis is given in Table 1, and consists  
92 primarily of SiO<sub>2</sub>, Al<sub>2</sub>O<sub>3</sub> and CaO. The high-calcium fly ash contains, approximately,  
93 52% of particles sized lower than 45 µm and 41% lower than 10 µm.

94 Speswhite kaolin provided by Imerys Minerals UK, and whose chemical composition is  
95 given in Table 1 was used. It is mainly constituted of kaolinite (95%) and secondarily of  
96 muscovite (4%) [3]. The kaolin contains, approximately, 100 % of particles sized lower  
97 than 10 µm and 80 % lower than 2 µm.

98 A unique alkaline solution was used: a sodium silicate with a mass ratio SiO<sub>2</sub>/Na<sub>2</sub>O of  
99 1.7 and a dry mass percentage of 44%; supplied by Woellner group and named GEOSIL  
100 34417.

101 Table 1

102 Chemical composition (wt. %) of raw fly ash and kaolin.

	SiO <sub>2</sub>	Al <sub>2</sub> O <sub>3</sub>	Fe <sub>2</sub> O <sub>3</sub>	CaO	CaO <sub>free</sub> <sup>a</sup>	MgO	SO <sub>3</sub>	Na <sub>2</sub> O	K <sub>2</sub> O	H <sub>2</sub> O	L.o.I.
Fly ash	39.4	19.8	7.4	18.6	5.2	1.8	4.1	2.0	1.8	0.0	1.7 <sup>b</sup>
Kaolin	49.2	34.5	1.2	0.0	0.0	0.2	0.0	0.1	1.7	13.1	12.0 <sup>c</sup>

103 <sup>a</sup> Free calcium oxide content, <sup>b</sup> from [3], <sup>c</sup> from [33]

104 *2.2 Sample preparation*

105 Sample preparation consisted in (i) mix of liquid sources ie. silicate and water (ii) mix  
106 of aluminosilicate powders ie. high-calcium fly ash and kaolin in the case of soil-source  
107 sample (iii) mix of (i) and (ii) previously prepared.

108 Three types of mixes were studied and named F100, KF50 and KF20. F100 is the high-  
109 calcium fly ash based alkali activated binder. It corresponds to a solid phase made of

110 high-calcium fly ash only, whereas KF50 and KF20 are the alkali activated soils. KF50  
111 corresponding to a solid phase made of 50% of high-calcium fly ash and 50% of kaolin  
112 in mass, and KF20 corresponding to a solid phase made of 20% of high-calcium fly ash  
113 and 80% of kaolin. List of samples is summarized up in Table 2.

114 To ensure a good workability, the amount of added water with respect to the solid mass  
115 (eg. mass of kaolin and high-calcium fly ash) was fixed to 50% for all the samples.  
116 Additionally, the mass ratio of alkaline solution to high-calcium fly ash was fixed to  
117 50% for all the samples, giving the initial molar ratios (considering that kaolin is  
118 unreactive): Si/Al = 2.0, Si/Na = 3.5 and Al/Na = 1.8. The Al/Na ratio was not fixed to  
119 one because of the presence of calcium ions in high quantity in our system playing a  
120 role of charge compensation as well as sodium.

121 The paste obtained was poured in closed plastic molds and cured at room temperature  
122 (20 °C). Samples were finally demoulded and freeze dried at curing times of 1, 3, 7 or  
123 28 days.

124 Table 2

125 Samples composition wt. %.

Sample	Fly ash	Kaolin	Water	Alkaline solution
F100	50	0	25	25
KF50	28.6	28.6	28.6	14.3
KF20	12.5	50	31.3	6.3

126  
127

### 128 *2.3 Methods*

129 A variety of characterisation techniques were complementary used to probe the  
130 mineralogical, structural and microstructural sample characteristics.



131 X-ray diffractograms of powdered samples were obtained with a Bruker D8 Advance  
132 diffractometer, using CuK $\alpha$  radiation generated at 40 mA and 40kV. Specimens were  
133 step-scanned from 2 to 60° 2 $\theta$  at 0.017° 2 $\theta$  steps integrated at the rate of 1s/step.

134 Derivative thermogravimetric curves were obtained on a Netzsch STA 449F3 Jupiter  
135 thermal analyser. The samples were heated from 20–1000 °C at a rate of 10 °C/min  
136 under argon atmosphere.

137 FTIR spectra were obtained on an FTIR Bruker Vertex 70 spectrometer. Specimens  
138 were prepared by mixing 30 mg of sample in 270 mg of KBr. Spectral analysis was  
139 performed over the range 4000–400 cm<sup>-1</sup> at a resolution of 4 cm<sup>-1</sup>.

140 Solid-state <sup>29</sup>Si NMR spectroscopy was performed using a Bruker Avance III 300 MHz  
141 (7 T) spectrometer and 7 mm MAS probe. <sup>29</sup>Si MAS spectra were acquired with a single  
142  $\pi/2$  pulse excitation of 5.5  $\mu$ s and <sup>1</sup>H decoupling. The repetition times were 2 s, 120 s  
143 and 30 s for the raw high-calcium fly ash, the raw kaolin and all the activated samples,  
144 respectively. For all <sup>29</sup>Si spectra, MAS spinning rate was set to 5 kHz. Solid-state <sup>27</sup>Al  
145 NMR spectroscopy was performed using a Bruker Avance III 500 MHz (11.7 T)  
146 spectrometer and 2.5 mm MAS probe. <sup>27</sup>Al MAS spectra were acquired with a single  
147 pulse excitation of  $\pi/12$  pulse of 3.3  $\mu$ s and <sup>1</sup>H decoupling. Repetition time was set to 1  
148 s and MAS spinning rate to 30 kHz. Spectra were referenced against TMS  
149 (tetramethylsilane) for <sup>29</sup>Si and an Al(NO<sub>3</sub>)<sub>3</sub> aqueous solution for <sup>27</sup>Al. Lastly, attention  
150 should be drawn to the fact that iron initially present in the high-calcium fly ash renders  
151 the interpretation more complex, notably spectra from different mixes cannot be  
152 quantitatively compared.

153 Finally, samples were studied by SEM from polished section. Freeze-dried samples  
154 were impregnated under a vacuum with an acrylic resin (LR White). The polymerisation

155 of the resin was performed in an oven at 60°C over 48 h. The samples were then  
156 polished with diamond powder and coated with carbon before the observation. The  
157 observations were done with a HITACHI SU5000 scanning electron microscope  
158 equipped with an energy-dispersive X-ray analyser (Quantax microanalyser system  
159 composed of X-Flash® SDD detector and the Esprit software). The microscope was  
160 operated at an accelerating voltage of 20 kV and working distances of 10 mm.

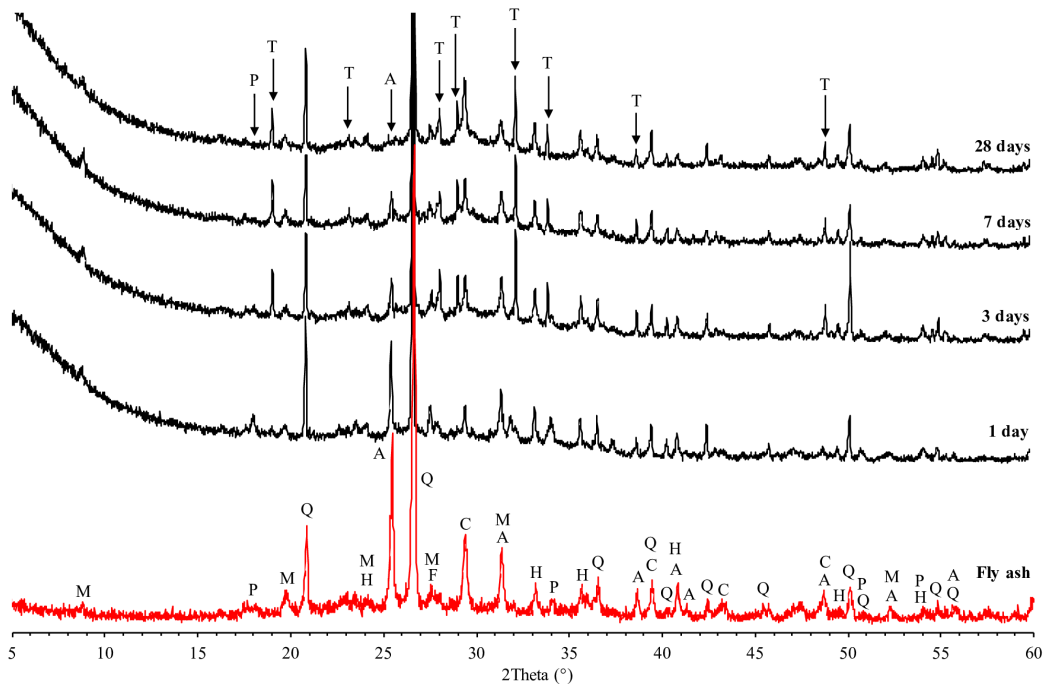
### 161 **3. Results and discussion**

162 The first section of results presents the physico-chemical evolution of the binder alone  
163 without the addition of kaolin. The second part focuses on the description of the soil  
164 source material mixed with binder. To end with, the system investigated in this study is  
165 compared with lime-based systems already described in the literature.

#### 166 *3.1 Alkali activated high-calcium fly ash binder*

##### 167 *3.1.1 X-ray diffraction (XRD)*

168 Results obtained by XRD show that the original high-calcium fly ash is constituted of a  
169 vitreous phase (hump between 17°2θ and 38°2θ), and crystalline phases which include  
170 calcium-containing minerals: anhydrite CaSO<sub>4</sub>, calcite CaCO<sub>3</sub> and portlandite Ca(OH)<sub>2</sub>,  
171 and other minerals: quartz SiO<sub>2</sub>, feldspar (K,Na,Ca)(Si,Al)<sub>4</sub>O<sub>8</sub>, hematite Fe<sub>2</sub>O<sub>3</sub> and  
172 muscovite (Si<sub>3</sub>Al)O<sub>10</sub>(Al<sub>2</sub>)(OH)<sub>2</sub>K (Fig. 1).



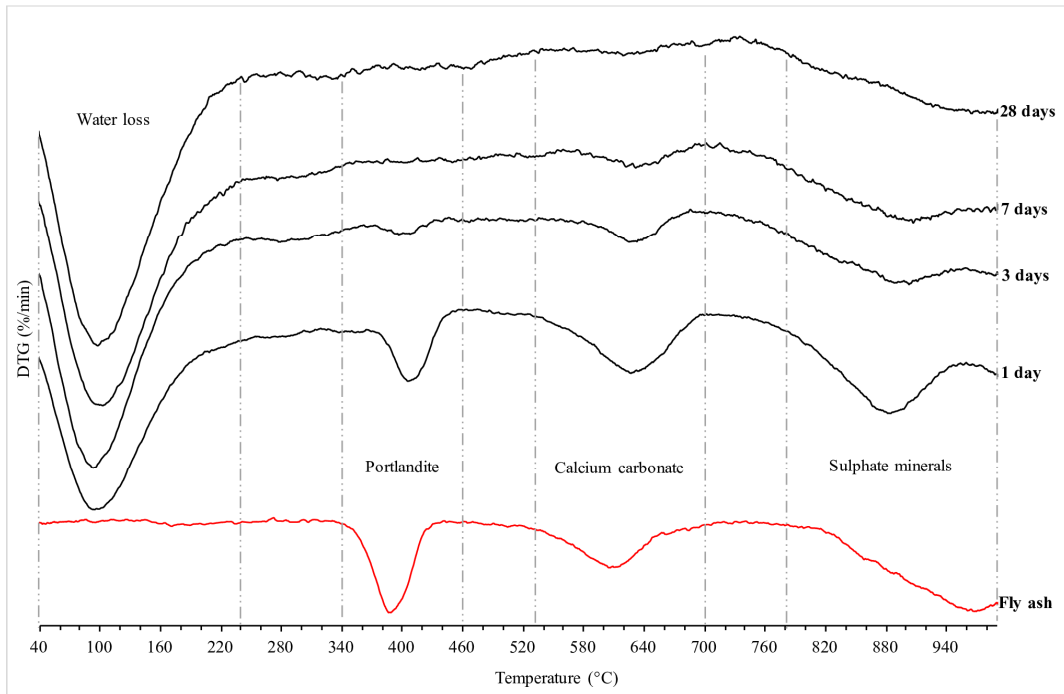
173

174 Fig. 1. XRD of raw fly ash and fly ash based alkali activated material F100 as a function of curing time; A=anhydrite;  
 175 C=calcite; F=feldspar; H=hematite; M=muscovite; P=portlandite; Q=quartz; T=thenardite.

176 Fig. 1 also shows XRD patterns of the alkali activated high-calcium fly ash as a  
 177 function of curing time. Regarding the crystalline phases, anhydrite  $\text{CaSO}_4$  and  
 178 portlandite  $\text{Ca}(\text{OH})_2$  are consumed as a function of time. In addition, thenardite  $\text{Na}_2\text{SO}_4$   
 179 starts forming at 3 days. Its formation can be explained by the release of sulphate anions  
 180 from anhydrite dissolution, and its subsequent combination with sodium issued from the  
 181 alkaline solution.

### 182 3.1.2 Derivative thermogravimetric analysis (DTG)

183 Fig. 2 shows derivative thermogravimetric analyses of the original high-calcium fly ash,  
 184 and the high-calcium fly ash based alkali activated binder as a function of time. The  
 185 DTG peaks of the original high-calcium fly ash detected at 385, 605 and 965 °C  
 186 indicate the decomposition of portlandite  $\text{Ca}(\text{OH})_2$ , calcium carbonate  $\text{CaCO}_3$  and  
 187 anhydrite  $\text{CaSO}_4$  respectively.



188

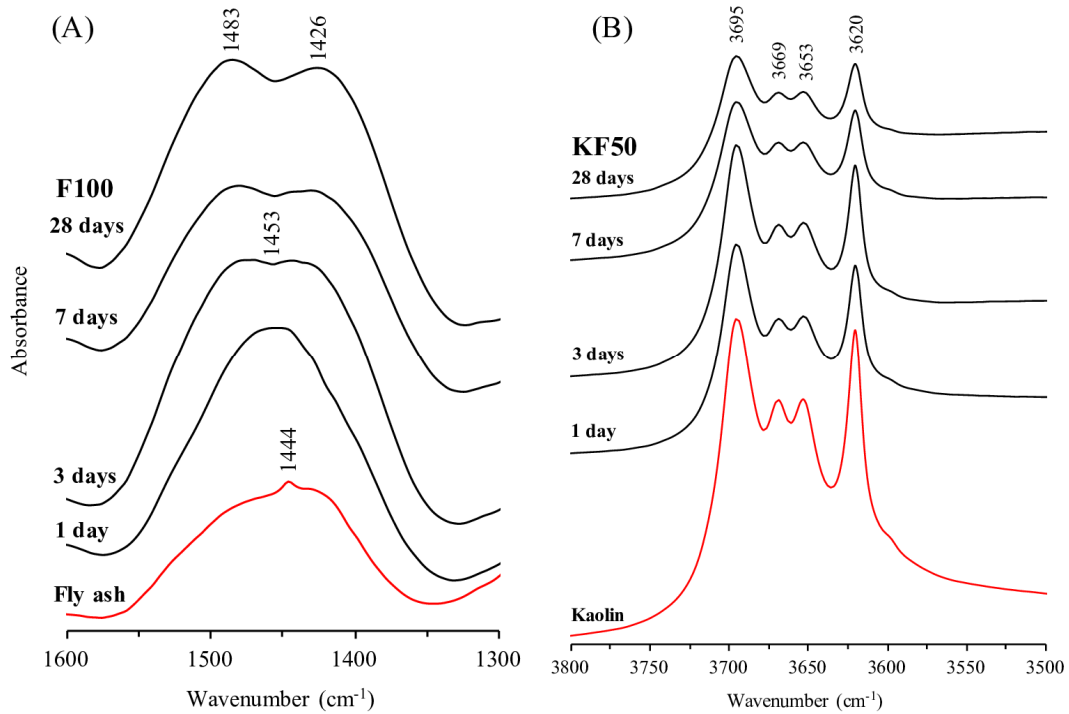
189 Fig. 2. DTG curves of raw fly ash and fly ash based alkali activated material F100 as a function of curing time.

190 The relatively low decomposition temperature of anhydrite compare to its theoretical  
 191 decomposition at 1214°C [31] is ascribed to the fact that anhydrite is found interlinked  
 192 with other calcium-rich phases by SEM (as illustrated later in section 3.1.4.1).

193 Regarding the alkali activated high-calcium fly ash, and complementary to XRD,  
 194 thermogravimetric analyses confirm the consumption of portlandite  $\text{Ca}(\text{OH})_2$  over time.  
 195 DTG curves also show the dissolution of calcium carbonate  $\text{CaCO}_3$  with time. Finally,  
 196 above 780 °C, the observed mass losses of the activated samples reveal the  
 197 decomposition of sulphate minerals: anhydrite  $\text{CaSO}_4$ , thenardite  $\text{Na}_2\text{SO}_4$  being formed  
 198 from 3 days as detected earlier by XRD (see 3.1.1), for which theoretical polymorphic  
 199 transformation occurs at around 900°C [32-33].

200 3.1.3 *Fourier Transform Infrared spectroscopy (FTIR)*

201 Fig. 3A shows FTIR spectra of the original high-calcium fly ash, and the high-calcium  
 202 fly ash based alkali activated binder as a function of time in the range of  $\text{CO}_3^{2-}$   
 203 stretching vibrations.



204  
 205 Fig. 3. FTIR of raw fly ash and fly ash based alkali activated material F100 as a function of curing time in the  $\text{CO}_3^{2-}$   
 206 stretching vibrations range (A) and raw kaolin and alkali activated kaolin KF50 as a function of curing time in the  
 207 OH stretching vibrations range (B).

208 Different features of the  $\text{CO}_3^{2-}$  band is observed over time: at 1 day a single band around  
 209 1453  $\text{cm}^{-1}$  is seen, while at 28 days a doublet positioned at 1426 and 1483  $\text{cm}^{-1}$  is  
 210 observed. Those modifications validate the formation of calcium carbonate during the  
 211 curing time as observed by DTG.

212 Finally, Fig. A.1 (see appendices) shows FTIR spectra in the area of sulphate minerals.  
 213 It confirms the dissolution of calcium sulphate (anhydrite,  $\text{CaSO}_4$ ) along with the  
 214 subsequent formation of sodium sulphate (thenardite,  $\text{Na}_2\text{SO}_4$ ) as previously seen by  
 215 XRD (see 3.1.1).

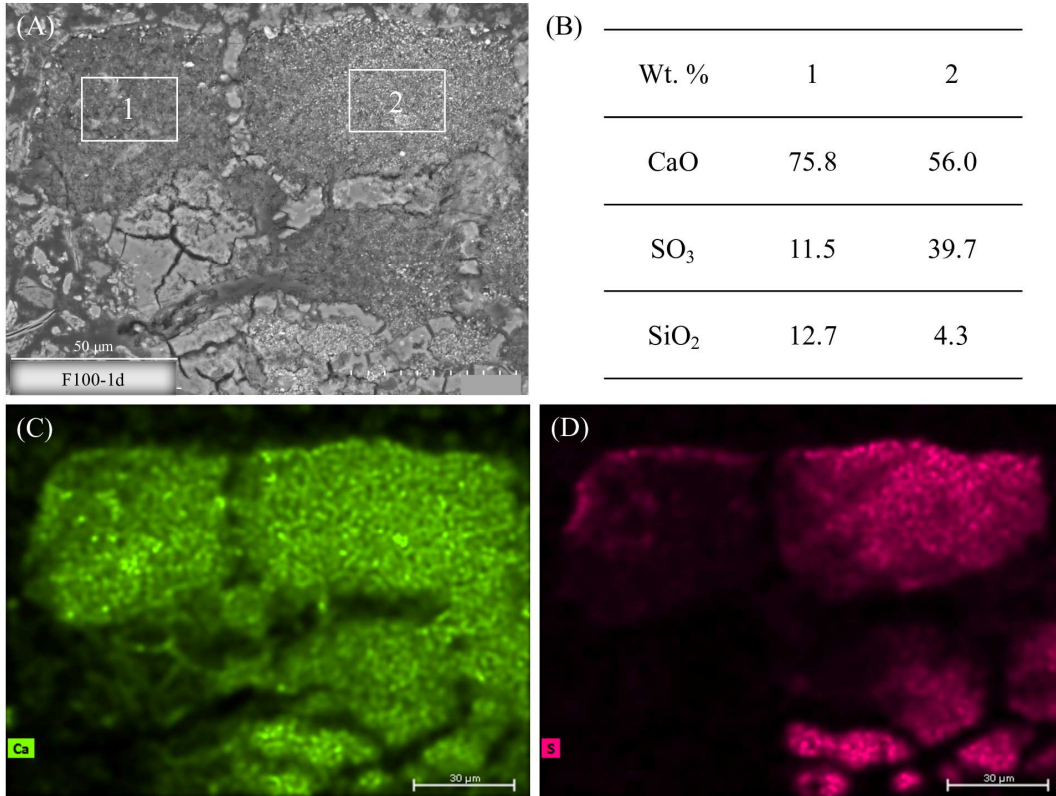
216 3.1.4 Scanning Electron Microscopy (SEM)

217 3.1.4.1 Calcium-rich phases

218 Fig. 4 shows SEM observations of the alkali activated high-calcium fly ash at 1 day.

219 More specifically, it focuses on calcium-rich phases previously detected as reactive  
220 phases being dissolved following the alkali attack by XRD, TGA and FTIR.

221 Calcium-rich phases are initially present in high-calcium fly ash as nodules of large size  
222 from 100 to 250  $\mu\text{m}$ . Besides, it is seen that chemical elements such as calcium, sulphur  
223 and silicon are not homogeneously spread within nodules suggesting a varying  
224 mineralogy. For instance, in area 2, despite a high content of sulphur indicating a  
225 prevalence of anhydrite ( $\text{CaSO}_4$ ), the detected percentage of  $\text{SO}_3$  with respect to  $\text{CaO}$   
226 remains too low to be owed to the presence of anhydrite phases only. It is therefore  
227 concluded that the various calcium-containing phases such as anhydrite  $\text{CaSO}_4$ , calcite  
228  $\text{CaCO}_3$  and portlandite  $\text{Ca}(\text{OH})_2$  (previously detected by XRD and DTG in section 3.1.1  
229 and 3.1.2) are interlaced within those nodule structures which represent reactive  
230 structures under alkaline attack.



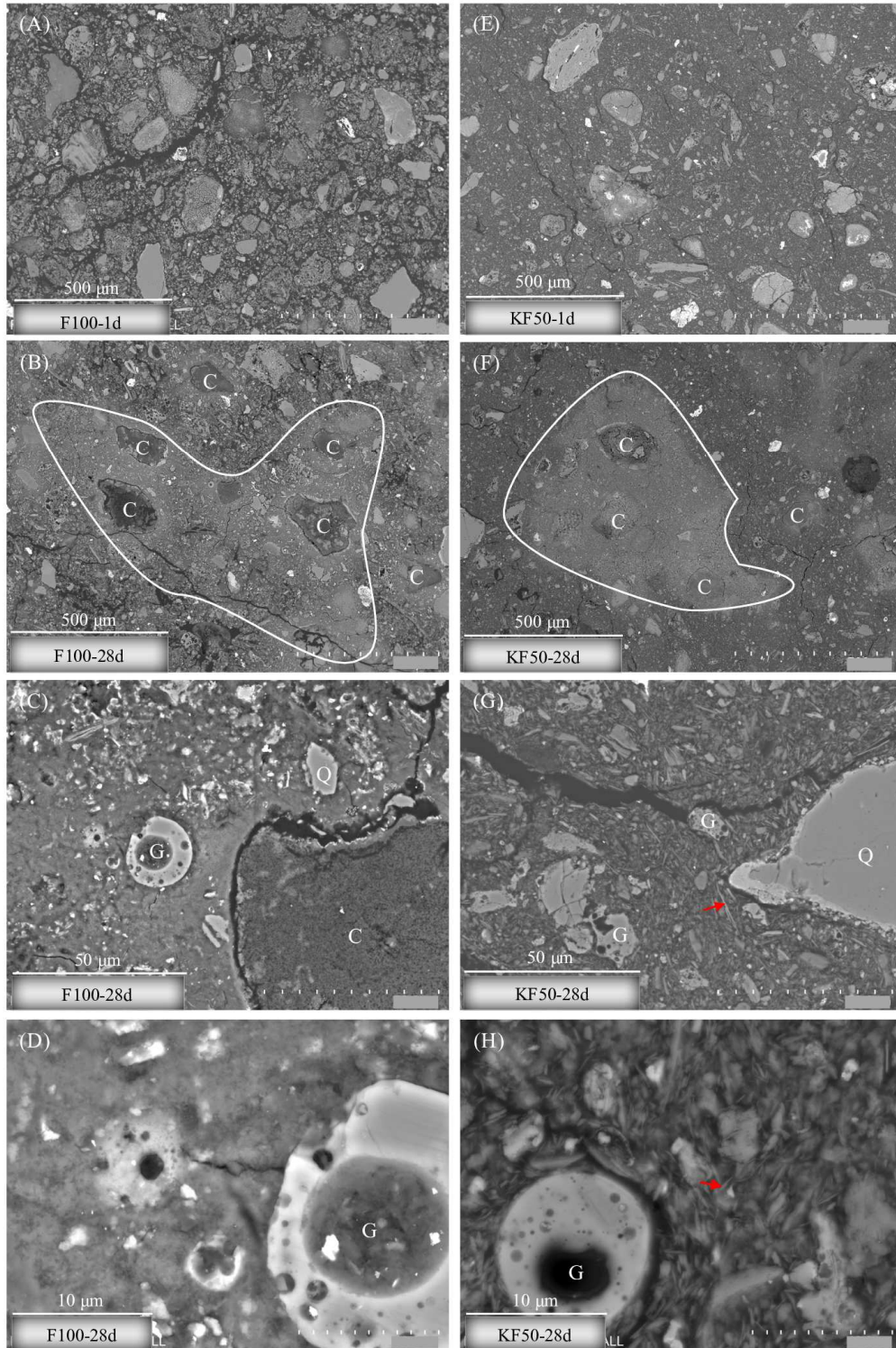
231

232 Fig. 4. SEM observations of a calcium-rich nodule from the alkali activated fly ash at 1 day: (A) SEM micrograph,  
 233 (B) chemical composition (wt. %) of areas 1 and 2, (C) and (D) chemical mappings of calcium and sulphur  
 234 respectively.

235 *Overall sample*

236 Fig. 5 additionally shows microstructural observations of the alkali activated high-  
 237 calcium fly ash binder. At 1 day (Fig. 5A), a porous material along with distinct  
 238 unreacted high-calcium fly ash particles is seen. In contrast, at 28 days (Fig. 5B), a more  
 239 compact material with less pores is observed evidencing the formation of new  
 240 compounds. Moreover, at 28 days, several unreacted high-calcium fly ash particles are  
 241 still observed especially from the vitreous phase i.e. spherical and vesicular particles  
 242 (see Fig. 5B, C and D).





243

244

245

246

Fig. 5. SEM micrographs of (i) the alkali activated fly ash binder F100 (Column 1) (A) at 1 day and (B), (C) and (D) at 28 days, (ii) the alkali activated kaolin KF50 (Column 2) (E) at 1 day and (F), (G) and (H) at 28 days; C=calcium nodules; G=glass; Q=quartz.



247 Additional chemical analyses revealed that changes in microstructure are more  
248 significant around calcium-rich particles which were previously detected as the main  
249 reactive part of the raw high-calcium fly ash.

250 As a matter of fact, SEM micrographs show zones of higher density appearing brighter  
251 around calcium-rich nodules (see encircled area in Fig. 5B).

252 Table 3 gives an average chemical composition of the denser reactive areas. Notably, it  
253 indicates a ratio of sodium to sulphur around 2 matching with that of precipitated  
254 thenardite whose formula is  $\text{Na}_2\text{SO}_4$ , and implying that most of the sodium from the  
255 alkaline solution is taken up to form thenardite.

256 Table 3

257 Average elemental composition (wt. %) of F100 and KF50 denser areas at 28 days.

	Si	Ca	Al	Na	S	K	Fe	Mg	O
F100-28d	22.1	19.2	7.0	3.7	1.7	1.2	0.8	0.5	43.8
KF50-28d	24.1	14.5	8.8	3.1	1.6	1.6	0.7	0.3	45.3

258

259 Furthermore, Table 3 indicates that the massive reactive area is primarily composed of  
260 silicon and calcium. Supposing that the new compounds are mainly located in those  
261 denser areas, these results suggest that apart from thenardite the new compounds are  
262 enriched in silicon and calcium.

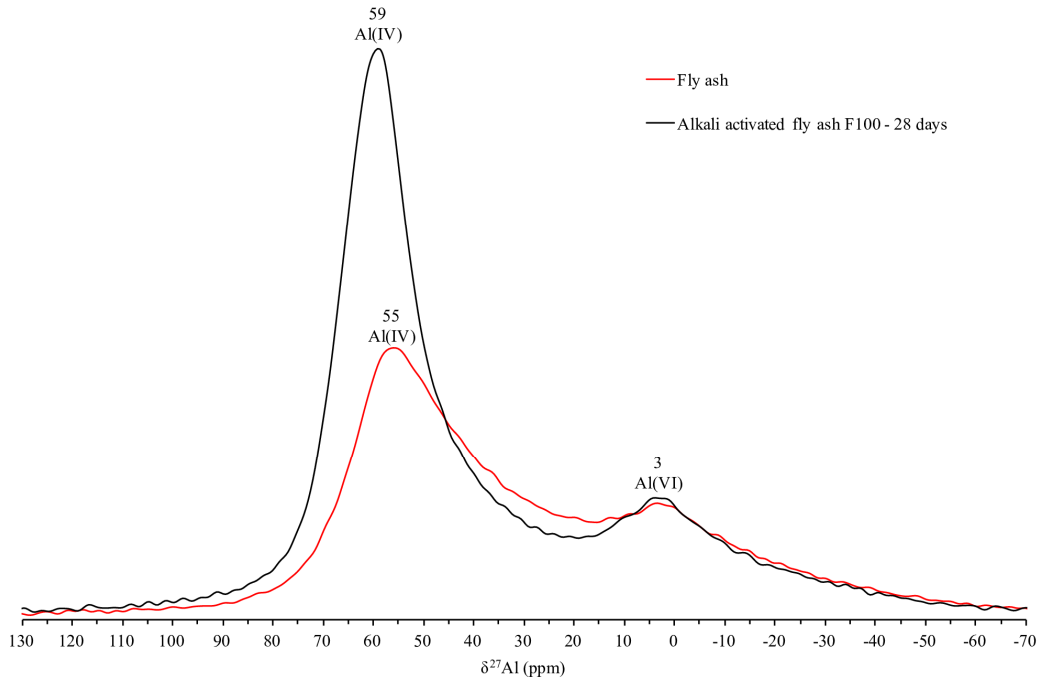
263

### 264 3.1.5 Nuclear Magnetic Resonance (NMR)

265 Nuclear Magnetic Resonance was finally used to follow amorphous phases and precise  
266 the structure of the new compounds formed in our investigated system.

267 Fig. 6 shows  $^{27}\text{Al}$  MAS-NMR spectrum of the original high-calcium fly ash as well as  
268 the spectrum belonging to the alkali activated high-calcium fly ash at 28 days.  $^{27}\text{Al}$   
269 NMR spectrum of the original high-calcium fly ash displays two resonances whose

270 dissymmetrical shapes are due to electric field gradient distribution caused by the  
271 distribution of geometries of the  $\text{AlO}_4$  and  $\text{AlO}_6$  polyhedra.. More specifically, the  
272 main resonance whose maximum is detected at 55 ppm corresponds to  $\text{Al(IV)}$  of the  
273 vitreous phase. While the resonance located at 3 ppm corresponds to  $\text{Al(VI)}$  of the  
274 vitreous phase.

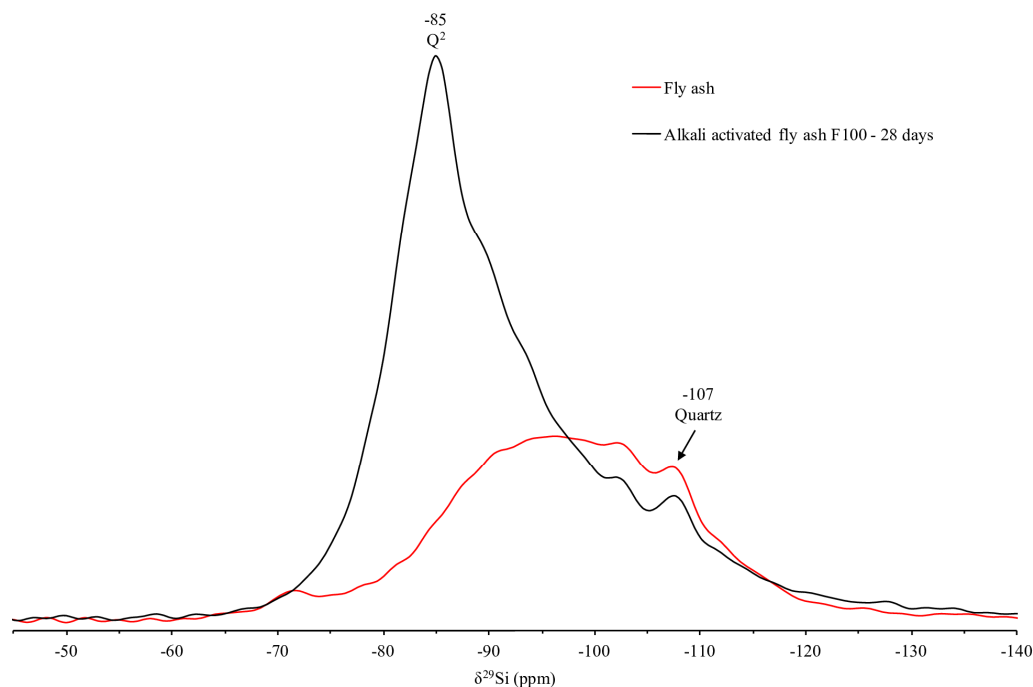


275  
276

Fig. 6.  $^{27}\text{Al}$  MAS-NMR spectra of the raw fly ash and alkali activated fly ash at 28 days.

277 Comparatively, the high-calcium fly ash based alkali activated material spectrum at 28  
278 days exhibits a main resonance sharper and a maximum shifted to 59 ppm  
279 corresponding to four-fold coordination of aluminium namely  $q^4(4\text{Si})$ . Those  
280 modifications in the spectrum compared to the original high-calcium fly ash indicate  
281 that part of the aluminium released from high-calcium fly ash leads to the formation a  
282 new aluminium bearing phase whose aluminium is tetrahedrally coordinated. Lastly, the  
283 resonance owed to octahedral aluminium at 3 ppm is still present which means that  
284 high-calcium fly ash is not totally dissolved after 28 days.

285 Fig. 7 shows  $^{29}\text{Si}$  MAS-NMR spectra of the original high-calcium fly ash as well as the  
286 alkali activated high-calcium fly ash at 28 days.  $^{29}\text{Si}$  NMR spectrum of the original  
287 high-calcium fly ash shows a broad resonance between -85 and -105 ppm attributed to  
288 the presence of a wide range of  $\text{Q}^3$  and  $\text{Q}^4$  silicon local environments from the vitreous  
289 phase.



290  
291

Fig. 7.  $^{29}\text{Si}$  MAS-NMR spectra of the raw fly ash and alkali activated fly ash at 28 days.

292 In contrast, the alkali activated high-calcium fly ash spectrum at 28 days displays a clear  
293 additional resonance centred at -85 ppm. This new position can be attributed to both the  
294 formation of  $\text{Q}^4(4\text{Al})$  or else  $\text{Q}^2$ -type silicon environments. Nevertheless, regarding the  
295 high value of the Si/Al ratio around 3.2 in the denser area comprising the new products,  
296 and measured by SEM (see Table 3) it is unlikely that  $\text{Q}^4(4\text{Al})$  environments are  
297 present. The new resonance at -85 ppm consequently indicates the formation of  $\text{Q}^2$ -type  
298 silicon environments in chain structure. Considering that the spectrum does not show  
299 any resonance corresponding to  $\text{Q}^1$  silicon environments the length of those formed  
300 chains is high. It is also worth noting that  $\text{Q}^2$  Si environments in chain possess a charge

301 deficit of 2- which must be compensated. However, sodium cations are not available as  
302 they are associated with sulphur to form thenardite  $\text{Na}_2\text{SO}_4$  (see sections 3.1.1 and  
303 3.1.3). Consequently, only calcium cations released from calcium reactive phases of  
304 high-calcium fly ash can compensate this charge deficit. Those silicon chain structures  
305 are therefore combined with dissolved calcium which matches with the chemical  
306 composition of the denser reactive area primarily made of silicon and calcium (see  
307 Table 2). The significant broadening of the resonance at -85 ppm also indicates that  
308 those chains are not well organised as C-S-H structures generally observed in Portland  
309 cement [34]. Considering the low Ca content of the raw fly ash, the line broadening  
310 fully agrees with amorphous C-S-H with a low Ca/Si ratio.

311 Finally, the broadest part of the activated high-calcium fly ash spectrum at 28 days from  
312 -90 ppm to -100 pm indicates the presence of  $\text{Q}^3$  and  $\text{Q}^4$  environments mainly issued  
313 from the remaining vitreous phase of high-calcium fly ash, and in accordance with the  
314 previous observations of unreacted high-calcium fly ash particles at 28 days by SEM  
315 (see 3.1.4.2).

316 In summary, both  $^{29}\text{Si}$  and  $^{27}\text{Al}$  MAS-NMR spectroscopy indicates the formation of  
317 new signals following alkaline activation. It is of interest to understand whether the new  
318 aluminium-containing phase seen in  $^{27}\text{Al}$  NMR correlates with the silicate chain  
319 structure observed in  $^{29}\text{Si}$  NMR. As a comparison, aluminium in linear structure such as  
320 C-S-H is either found (i) as  $\text{Q}^2$  environments corresponding to aluminium substituting  
321 for silicon atoms, and located around 68-74 ppm in  $^{27}\text{Al}$  NMR or else (ii) as  $\text{Q}^3$   
322 environments corresponding to crosslinking through alumina bridging tetrahedra  
323 positioned around 63-68 ppm in  $^{27}\text{Al}$  NMR [35-37]. However, as mentioned above, the  
324 new aluminium resonance observed in our investigation at 59 ppm would rather

325 correspond to  $q^4(4Si)$  environment. Consequently, if aluminium is incorporated into the  
326 silicate chain structure, it would be in a three-dimensional environment which has not  
327 been described in literature yet. To conclude, results concerning the alkali activated  
328 high-calcium fly ash binder showed that calcium-rich phases constitute the reactive part  
329 of the raw high-calcium fly ash, while its vitreous phase remains mainly unreactive. The  
330 new compounds formed are mainly located around calcium-rich reactive particles and  
331 present a complex chemistry and structure which differ from cementitious compounds  
332 generally encountered in cement or lime based system.

333

### 334 *3.2 Interaction between the alkali activated high-calcium fly ash binder and kaolin*

335 The following section aims at understanding the interaction between kaolin and the  
336 alkali activated high-calcium fly ash binder previously described. More specifically, it  
337 aims at answering the following question: does the presence of kaolin modify the  
338 reaction sequence?

339 Two stabilised soils were studied i.e. KF50 for which the solid phase is made in mass of  
340 50% of high-calcium fly ash and 50% of kaolin, and KF20 made of 20% of high-  
341 calcium fly ash and 80% of kaolin. Observations made for these two mixes turned out to  
342 be similar for all the techniques used. Therefore, only the results of KF50 will be shown  
343 while the results of KF20 can be found in Supporting Information.

344

345 Firstly, Fig. 3B shows the infrared spectrum of the original kaolin as well as the spectra  
346 belonging to the alkali activated soil KF50 as a function of time. The four bands  
347 observed in the  $3695\text{--}3620\text{ cm}^{-1}$  range are typical of the presence of kaolinite, and arise  
348 from the vibration of its internal OH groups. Notably, disorder in kaolinite is mainly

349 detectable in this OH-stretching region by FTIR [38]. Those bands being still observed  
350 over time in the alkali activated soils suggest that kaolinite does not react under alkaline  
351 conditions. The smaller heights seen at 7 and 28 days are only due to higher sample  
352 densities at higher curing times after the formation of new compounds, leading to  
353 smaller probed distance and therefore lesser absorbance.

354

355 Fig. A.3 (see appendices) shows XRD patterns of the activated soil KF50 as a function  
356 of curing time. Similarly to the alkali activated high-calcium fly ash binder (see 3.1.1),  
357 it indicates the dissolution of anhydrite  $\text{CaSO}_4$  along with the formation of thenardite  
358  $\text{Na}_2\text{SO}_4$ .

359

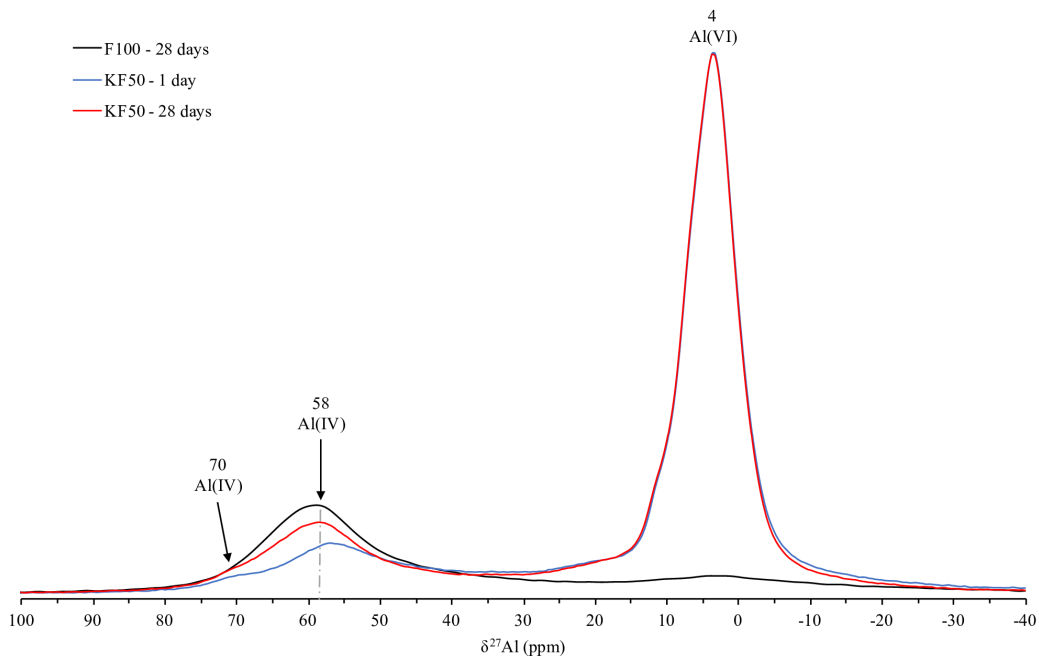
360 Fig. 5E, F, G and H shows microstructural observations of the alkali activated kaolin  
361 KF50. At 1 day, and in contrast with the alkali activated high-calcium fly ash (Fig. 5A),  
362 KF50 presents a relatively low porosity due to the presence of small-sized kaolinite  
363 platelets filling the pores (Fig. 5E). At 28 days, and in a similar way to the activated  
364 high-calcium fly ash (Fig. 5B), KF50 presents a more compact microstructure around  
365 calcium-rich phases (see encircled area in Fig. 5F).

366 Furthermore, by comparing the alkali activated high-calcium fly ash binder (Fig. 5C and  
367 D) with the activated soil KF50 (Fig. 5G and H), kaolinite platelets are distinctly  
368 observed (see red arrows as an example of platelet observation), and homogeneously  
369 spread across the whole sample. In fact, kaolinite platelets were observed not merely in  
370 the matrix but also in the most reactive massive areas supporting that kaolinite does not  
371 react even in the reactive areas but rather acts as a filler.

372 Table 2 gives an average chemical composition of KF50 massive areas. It shows similar  
373 tendencies than for the alkali activated high-calcium fly ash binder F100. Only slightly  
374 higher contents of silicon and aluminium are measured for KF50 due to the presence of  
375 kaolinite.

376 Fig. 8 shows  $^{27}\text{Al}$  MAS-NMR spectra of the alkali activated high-calcium fly ash binder  
377 F100 studied in the first section, and the alkali activated soil KF50 at 1 and 28 days. By  
378 comparison with the binder F100,  $^{27}\text{Al}$  NMR spectroscopy of KF50 displays two  
379 additional resonances due to the presence of kaolin i.e. a main resonance at 4 ppm due  
380 to Al(VI) of the octahedral layer of kaolinite, and a resonance at 70 ppm owed to Al(IV)  
381 and corresponding to substitution of Al for Si in the tetrahedral layer of kaolinite and  
382 muscovite.

383 At 1 day, KF50 presents a resonance whose maximum is located at 55 ppm and owed to  
384 the vitreous phase of high-calcium fly ash, while at 28 days a shift of this resonance to  
385 58 ppm indicates the formation of tetrahedral aluminium in  $q^4(4\text{Si})$  environments (as  
386 previously described for the alkali activated high-calcium fly ash in section 3.1.5).



387

388 Fig. 8.  $^{27}\text{Al}$  MAS-NMR spectra of the alkali activated fly ash F100 at 28 days and alkali activated kaolin KF50 at 1  
389 and 28 days.

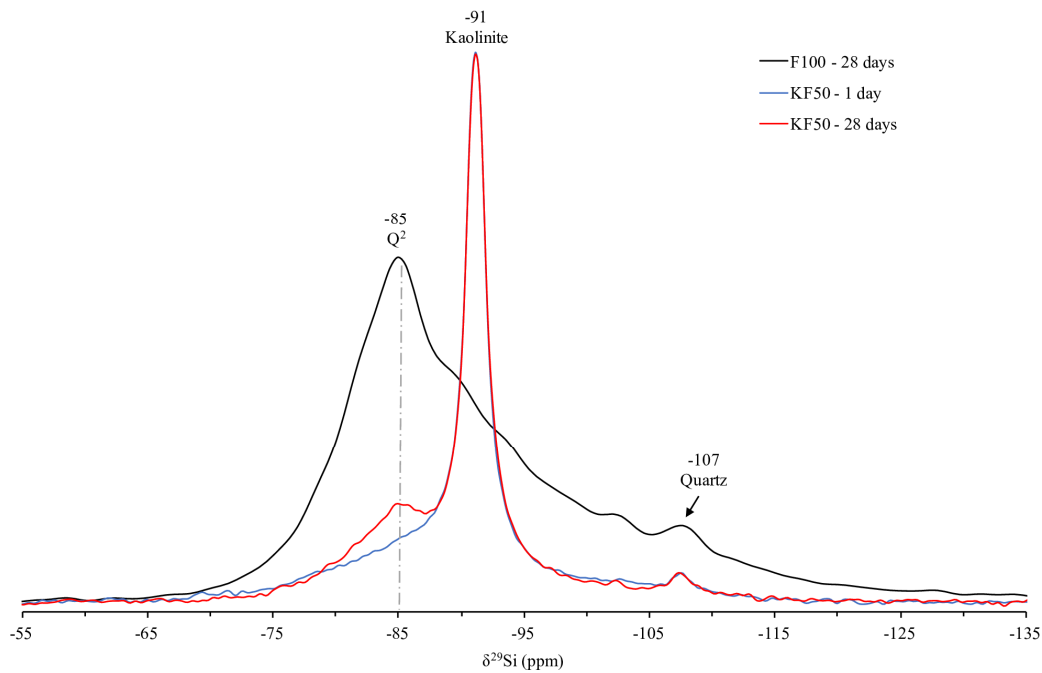
390 Fig. 9 shows  $^{29}\text{Si}$  MAS-NMR spectra of the alkali activated high-calcium fly ash binder  
391 F100 studied in the first section, and the alkali activated soil KF50 at 1 and 28 days.  $^{29}\text{Si}$   
392 NMR spectroscopy of KF50 samples show an additional thin resonance at -91 ppm  
393 corresponding to the silicon of the tetrahedral layer of kaolinite. This resonance does  
394 not undergo any modification over time confirming the non-reactivity of kaolinite.

395 Furthermore, from 1 to 28 days KF50 shows the clear appearance of a resonance at -85  
396 ppm due to the formation of silicon chains combined with dissolved calcium, and as  
397 previously described for the alkali activated high-calcium fly ash binder (see 3.1.5).

398

399 To conclude, results of this second section showed that kaolin is unreactive during  
400 alkaline attack. Besides, a similar reaction sequence than for the alkali activated high-  
401 calcium fly ash binder occurs.





402  
403

Fig. 9.  $^{29}\text{Si}$  MAS-NMR spectra of the alkali activated fly ash F100 at 28 days and alkali activated kaolin KF50 at 1 and 28 days.

404

405

### 406 3.3 Comparison with lime treated kaolin

407 This last section focuses on a comparison with previous studies which reported the  
408 physicochemical evolution of the same kaolin treated either by a common stabiliser:  
409 lime [6], but also treated by a mix of lime and the high-calcium fly ash used here [39].

410 Table 4 gives a summary of the reaction sequences for each system highlighting strong  
411 differences. This section consequently aims at providing a better understanding of the  
412 consequences of those variable reaction sequences on the final material in terms of  
413 performance and durability.

414 Table 4

415 Compared reactivity sequences of kaolin treated either by lime, or a mix of lime and fly ash or an alkali  
416 activated fly ash

	<b>Kaolin + Lime [6]</b>	<b>Kaolin + Lime + Fly ash [33]</b>	<b>Kaolin + Alkali activated fly ash</b>
--	--------------------------	-------------------------------------	--

1. Phases dissolved		Kaolin, lime	Kaolin, lime, fly ash	Fly ash
2. Reactivity timescale		Slow	Fast	Fast
3. Phases formed	Aluminate	Calcium Aluminate Hydrate C-A-H Monocarboaluminate hydrate C <sub>4</sub> -A-C-H <sub>11</sub>	Calcium Aluminate Hydrate C-A-H Calcium Aluminium Oxide Carbonate Hydrate C-A-O-C-H Calcium Aluminium Oxide Hydrate C-A-O-H Ettringite Ca <sub>6</sub> Al <sub>2</sub> (SO <sub>4</sub> ) <sub>3</sub> (OH) <sub>12</sub> .26H <sub>2</sub> O	Amorphous silicate consisting of chains combined with calcium - and probably incorporating the observed q4(4Si) aluminium environments
	Silicate	None	Calcium Silicate Hydrate C-S-H	

417

### 418 3.3.1 Reactivity of initial phases

419 Firstly and regarding the reactivity of the phases initially present, it was found that  
420 kaolin is inert in our alkali activated samples which contrasts with the two other lime  
421 based systems for which kaolinite is dissolved. The limited reactivity of kaolinite in the  
422 alkali activated soils herein studied is due to the presence of other more reactive phases.  
423 Besides, its limited reactivity is beneficial for the system as no side effects will occur.  
424 For the three systems, calcium-containing phases constitute the main reactive part of the  
425 mixes playing a pivotal role in the reaction development scheme. In fact, their  
426 dissolution leads to the release of dissolved calcium into the medium and hence  
427 pozzolanic activity i.e. formation of new calcium cementitious compounds responsible  
428 of the strength improvement. In the case of our alkali activated soils however, it is not  
429 lime CaO that constitutes a supply of calcium but calcium-containing minerals from  
430 high-calcium fly ash CaSO<sub>4</sub>, CaCO<sub>3</sub> or Ca(OH)<sub>2</sub>. For all calcium-source types the  
431 supply of Ca<sup>2+</sup> cations remains identical. What changes is the anion simultaneously  
432 released from their dissolution: when high-calcium fly ash is present the dissolution of  
433 its calcium-containing minerals is accompanied by the release of various anions such as

434 OH,  $\text{SO}_4^{2-}$  and  $\text{CO}_3^{2-}$  influencing the reaction sequence, and with potential negative  
435 effects for the durability as seen later.

436 Finally, concerning the vitreous phase of high-calcium fly ash, although amorphous and  
437 hence metastable it showed few reactivity leading to a preferential pozzolanic activity  
438 as seen in Portland cement, rather than polymerisation reactions associated with the  
439 formation of an aluminosilicate three-dimensional network characteristic of low-  
440 calcium alkali activated materials and geopolymers.

### 441 *3.3.2 Reactivity timescale*

442 Reactions in presence of high-calcium fly ash are fast with new compounds already  
443 observed at 28 days for both systems made of kaolin, lime and high-calcium fly ash [39]  
444 but also kaolin and alkali activated high-calcium fly ash. Whereas, longer reactivity  
445 timescale occurs for lime treated kaolin: new cementitious compounds being previewed  
446 from 60 days and clearly detected only after 270 days [6].

447 For a system made of lime and kaolin its pozzolanic activity depends on the dissolution  
448 of kaolinite which constitutes the only source of aluminium and silicon. Considering  
449 that kaolinite possesses a stable crystalline mineral structure hard to dissolve it explains  
450 the slow reactivity of that system. By contrast, high-calcium fly ash contains reactive  
451 phases i.e. calcium-rich phases primarily and to a small extent its vitreous phase (for the  
452 high-calcium fly ash used here) thermodynamically less stable than kaolinite and  
453 therefore easier to dissolve. That is why reaction sequences are faster for both high-  
454 calcium fly ash systems. It is even faster for our alkali activated soils as the alkaline  
455 solution brings a mixture of ions ready available. Those fastest reaction times would  
456 constitute an advantage in the case where the quickly formed products are as well stable  
457 binding phases which will be discussed now.

458 3.3.3 *Stability and structure of the compounds formed*

459 In the case of formerly studied systems made of kaolin and lime as well as kaolin, lime  
460 and high-calcium fly ash, a preferential release of aluminium over silicon from kaolinite  
461 and/or high-calcium fly ash dissolution occurs conducting to the formation of  
462 aluminium compounds primarily. In fact, for a lime treated kaolin Calcium Aluminate  
463 Hydrate C–A–H and monocarboaluminate hydrate  $C_4\text{--}A\text{--}C\text{--}H_{11}$  are formed [6]. In the  
464 case of a kaolin treated by a mix of lime and high-calcium fly ash Calcium Aluminate  
465 Hydrate C–A–H but also Calcium Aluminium Oxide Carbonate Hydrate C–A–O–C–H,  
466 Calcium Aluminium Oxide Hydrate C–A–O–H and Ettringite  
467  $\text{Ca}_6\text{Al}_2(\text{SO}_4)_3(\text{OH})_{12}\cdot 26\text{H}_2\text{O}$  are formed [39]. Whereas, in our alkali activated soils  
468 investigated here, aluminium dissolved from the vitreous phase of high-calcium fly ash  
469 was found in a three-dimensional four-fold environment ( $q^4(4\text{Si})$ ) which strongly  
470 contrasts with the six-fold environments found in the Calcium Aluminate Hydrates.  
471 Regarding the formation of silicate compounds, none are formed in a system made of  
472 kaolin and lime [6] because the dissolution of kaolinite is slow and starts by the release  
473 of its aluminium. Hence, no silicon is made available. Kaolinite being the only source of  
474 silicon in that system the limited dissolution of silicon implies the non-formation of  
475 silicon compounds. By contrast in a kaolin, lime and high-calcium fly ash system, the  
476 dissolution of silicon from the vitreous phase of high-calcium fly ash leads to the  
477 formation of Calcium Silicate Hydrate C–S–H [39]. Finally, in the alkali activated soils  
478 herein studied, the supply of silicon from the alkaline solution primarily and also from  
479 the vitreous phase of high-calcium fly ash leads to the formation of silicon chains  
480 combined with calcium, but whose NMR signature greatly differs from C–S–H  
481 commonly observed as described above (see section 3.1.5). It is also likely that

482 aluminium found in three-dimensional four-fold environment ( $q^4(4Si)$ ) is incorporated  
483 into those silicon chains.

484 Calcium Silicate Hydrate C–S–H is the principal binding phase of Portland cement and  
485 concrete primarily responsible for its strength [40]. In addition, its structure is more  
486 stable than Calcium Aluminate Hydrates [41]. Their presence is consequently beneficial  
487 for the performances. The fact that in our alkali activated samples, a diverse structure  
488 compared to usual C–S–H is observed cannot easily be assessed in term of stability at  
489 the present moment. Indeed, regarding the lack of crystallinity of our silicon chains  
490 formed, experience proved that the crystallinity of the binding agent alone constitutes a  
491 poor measure of stability over the timescales relevant to the majority of concrete  
492 structures [41]. A further investigation of the performances would help apprehending a  
493 potential beneficial effect of this uncommon silicon chains structure over time.

494

495 Finally, for both high-calcium fly ash systems, sulphate minerals are formed: either  
496 Ettringite  $Ca_6Al_2(SO_4)_3(OH)_{12}.26H_2O$  for a system made of kaolin, lime and high-  
497 calcium fly ash [39], or Thenardite  $Na_2SO_4$  in our alkali activated soils.

498 Their formation is due to the dissolution of anhydrite  $CaSO_4$  initially present in the  
499 high-calcium fly ash, and releasing sulphate anions  $SO_4^{2-}$  that are subsequently  
500 recombining with available cations. For the case of a kaolin, lime and high-calcium fly  
501 ash system the formation of Ettringite is taking up aluminium and calcium hence  
502 slowing down both the simultaneous formation of aluminate and silicate hydrates.  
503 Whereas, in our alkali activated system, sodium cations ready available from the  
504 alkaline solution combine with sulphate anions. Therefore, the formation of sulphate  
505 minerals does not affect the parallel development of the pozzolanic activity i.e. the

506 formation of silicate chains. Finally, a key point to consider for durability aspects is the  
507 high solubility of sulphate minerals which are few stable salts in water. In fact, a  
508 previous study in which leaching tests were performed on an alkali activated sulphate-  
509 bearing kaolin showed that the uptake of sulphate anions by the gel is low, namely less  
510 than 40% [42]. The study of the effect of wetting-drying cycles is consequently  
511 warranted to verify a further impact of the presence of thenardite on the long-term  
512 performances.

### 513 **3 Conclusions**

514 Here, the development of a novel soil binder that is an alkali activated calcium-rich  
515 high-calcium fly ash for clay soil stabilisation was explored. The study of its reactivity  
516 showed that (i) the overall calcium-bearing minerals from high-calcium fly ash  
517 constitute the reactive phases while its vitreous phase remains mainly unreactive, (ii)  
518 new compounds are formed, thenardite  $\text{Na}_2\text{SO}_4$  and an amorphous silicate consisting of  
519 chains combined with calcium - (iii) reactions happen within 1 to 28 days.

520 The interaction between the binder developed and the model soil chosen i.e. kaolin,  
521 showed that kaolin is unreactive. Its presence whatever the proportion does not modify  
522 the physicochemical evolution of the system that is neither the dissolved phases, formed  
523 compounds, nor reactivity timescale. The inert kaolinite platelets were in addition found  
524 homogenously embedded in the matrix acting as a filler.

525 When compared to lime treated kaolin, although pozzolanic activity remains the  
526 dominant process reaction sequences are strongly different. In the case of alkali  
527 activated soils the formation of calcium-silicon chains phases more stable than calcium  
528 aluminium hydrates encountered in lime based systems is beneficial for long-term  
529 stability purpose. Those observed silicon chains however show an uncommon structure

530 whose effect on the performances will be checked in a future investigation. Finally, the  
531 formation of thenardite a highly soluble salt in water raises interest about the durability  
532 of the material which will be also further investigated.

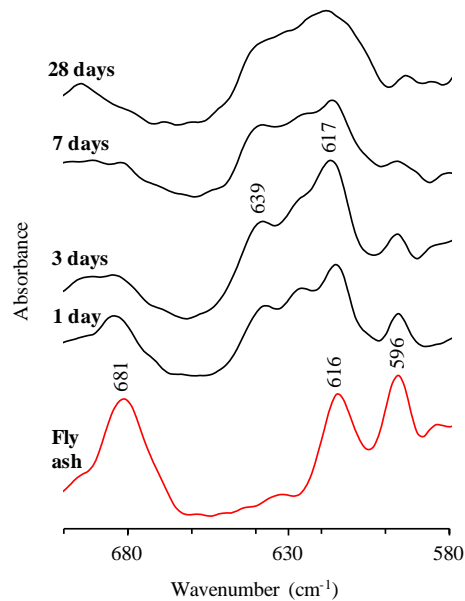
533

#### 534 **Acknowledgements**

535 The authors wish to acknowledge the support of the European Commission via the  
536 Marie Skłodowska-Curie Innovative Training Networks (ITN-ETN) project TERRE  
537 'Training Engineers and Researchers to Rethink geotechnical Engineering for a low  
538 carbon future' (H2020-MSCA-ITN-2015-675762).

539

#### 540 **Appendices**

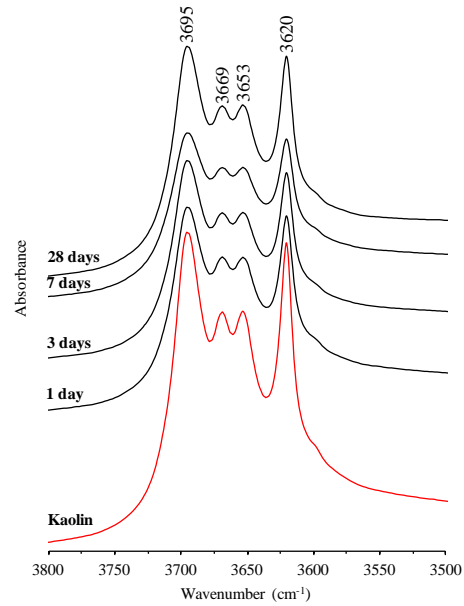


541

542 Fig. A.1. FTIR of raw high-calcium fly ash, and high-calcium fly ash based alkali  
543 activated material F100 as a function of curing time in the  $\text{SO}_4^{2-}$  stretching vibrations  
544 range; 681, 616 and 596  $\text{cm}^{-1}$  = anhydrite  $\text{CaSO}_4$ ; 639 and 617  $\text{cm}^{-1}$  = thenardite

545



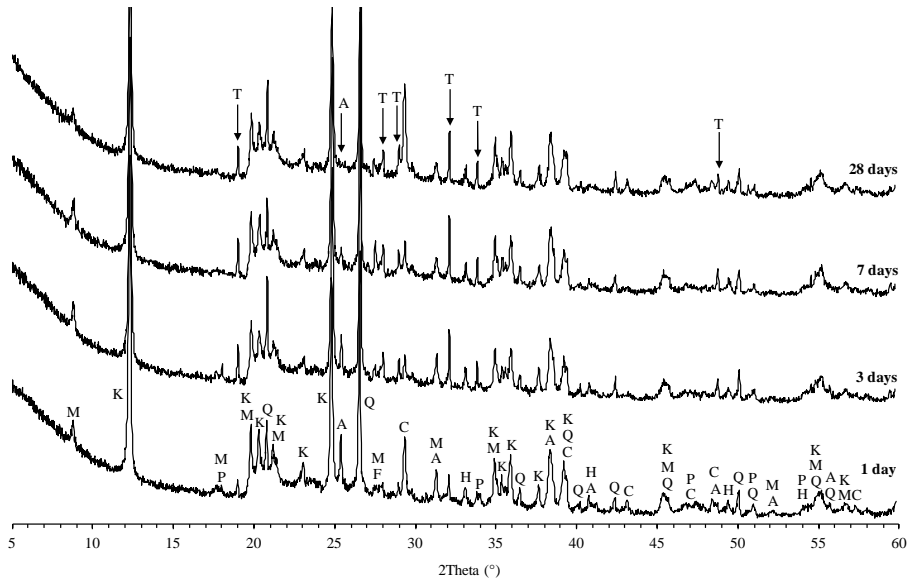


546

547 Fig. A.2. FTIR of the raw kaolin and alkali activated kaolin KF20 as a function of

548

curing time in the OH stretching vibrations range.



549

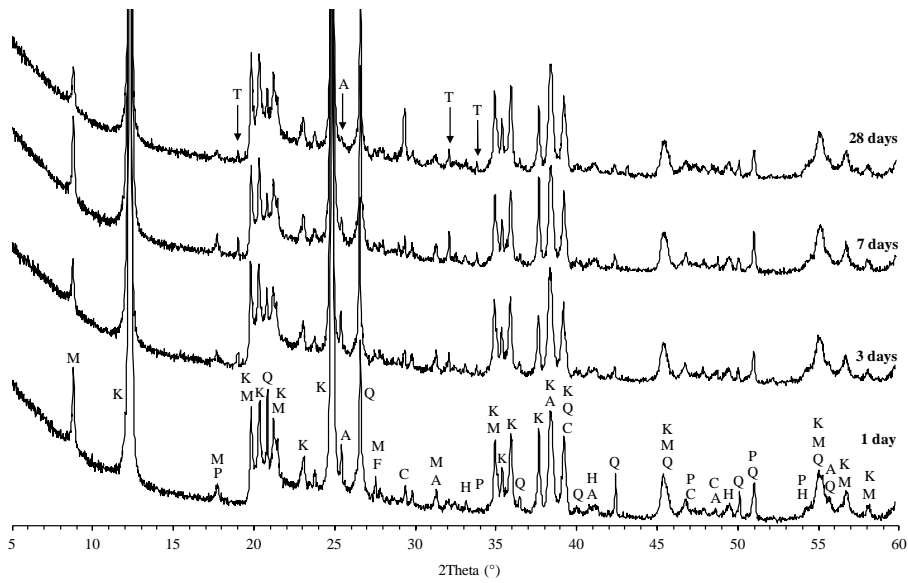
550 Fig. A.3. XRD of alkali activated kaolin KF50 as a function of curing time;

551 A=anhydrite; C=calcite; F=feldspar; H=hematite; K=kaolinite; M=muscovite;

552

P=portlandite; Q=quartz; T=thenardite.



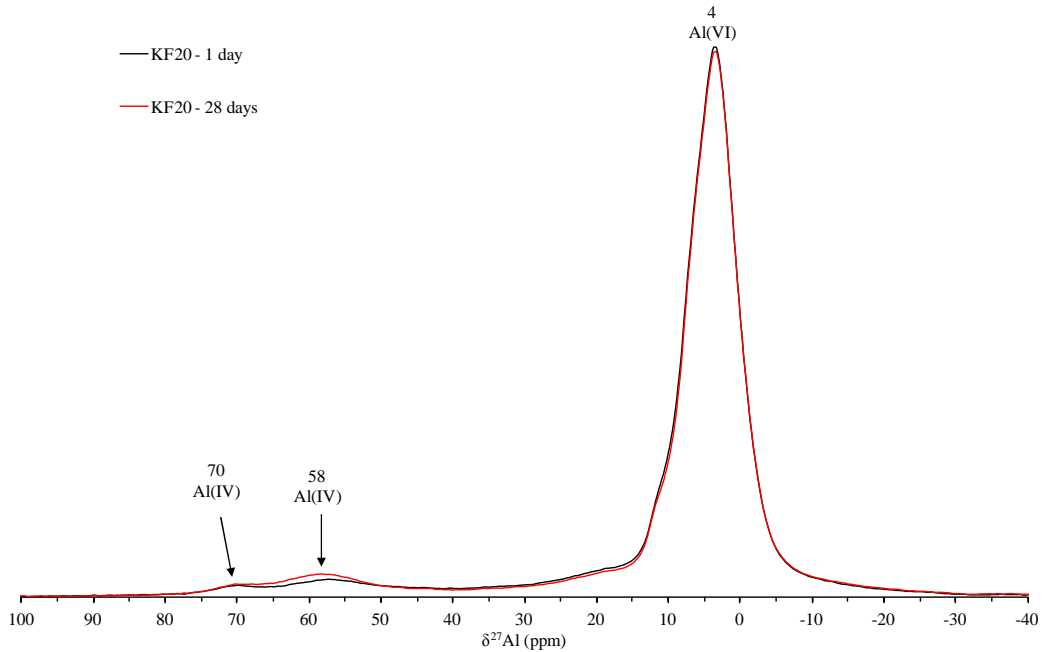


553

554 Fig. A.4. XRD of the alkali activated kaolin KF20 as a function of curing time;

555 A=anhydrite; C=calcite; F=feldspar; H=hematite; K=kaolinite; M=muscovite;

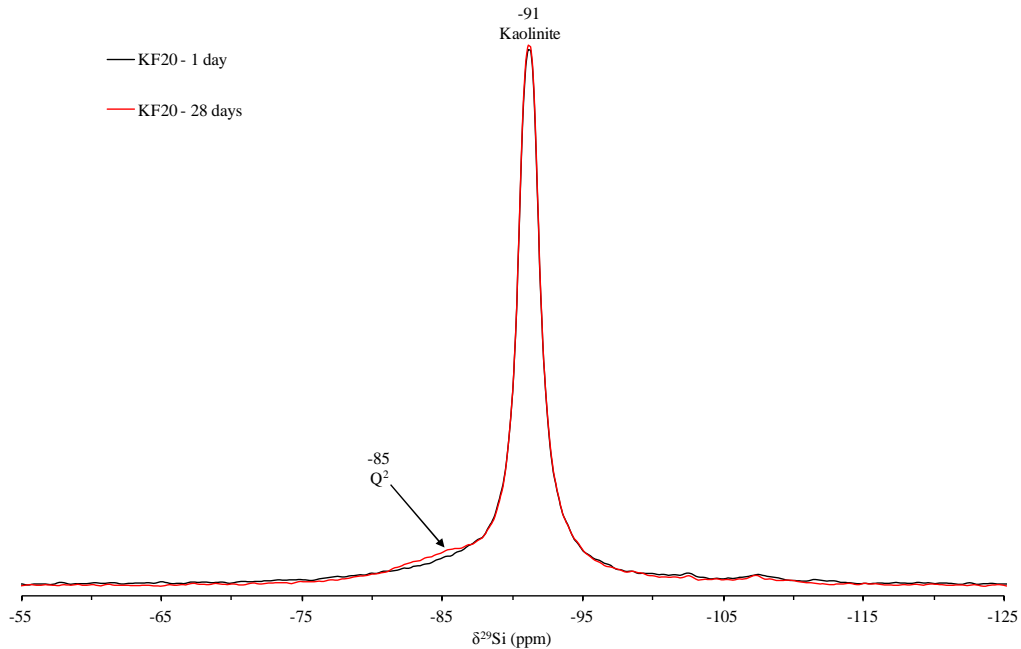
556 P=portlandite; Q=quartz; T=thenardite.



557

558 Fig. A.5. <sup>27</sup>Al MAS-NMR of the raw high-calcium fly ash, raw kaolin and alkali

559 activated kaolin KF20 at 0 and 28 days.



560

561 Fig. A.6.  $^{29}\text{Si}$  MAS-NMR of the raw high-calcium fly ash, raw kaolin and alkali

562 activated kaolin KF20 at 0 and 28 days.

563

564

## 565 References

566 [1] Pomakhina, E., Deneele, D., Gaillot, A.-C., Paris, M., Ouvrard, G., 2012.  $^{29}\text{Si}$  solid  
 567 state NMR investigation of pozzolanic reaction occurring in lime-treated Ca-bentonite.  
 568 *Cem. Concr. Res.* 42, 626–632.

569

570 [2] Lemaire, K., Deneele, D., Bonnet, S., Legret, M., 2013. Effects of lime and cement  
 571 treatment on the physicochemical, microstructural and mechanical characteristics of a  
 572 plastic silt. *Eng. Geol.* 166, 255–261.

573

574 [3] Chemed, Y.C., Deneele, D., Christidis, G.E., Ouvrard, G., 2015. Influence of  
 575 hydrated lime on the surface properties and interaction of kaolinite particles. *Appl. Clay  
 576 Sci.* 107, 1–13.

577

578 [4] Deneele, D., Le Runigo, B., Cui, Y. J., Cuisinier, O., Ferber, V., 2016. Experimental  
 579 assessment regarding leaching of lime-treated silt. *Constr. Build. Mater.* 112, 1032–  
 580 1040.

581

582 [5] Maubec, N., Deneele, D., Ouvrard, G., 2017. Influence of the clay type on the  
 583 strength evolution of lime treated material. *Appl. Clay Sci.* 137, 107–114.

584  
585 [6] Vitale, E., Deneele, D., Paris, M., Russo, G., 2017. Multi-scale analysis and time  
586 evolution of pozzolanic activity of lime treated clays. *Appl. Clay Sci.* 141, 36–45.  
587  
588 [7] Guidobaldi, G., Cambi, C., Cecconi, M., Deneele, D., Paris, M., Russo, G., Vitale,  
589 E., 2017. Multi-scale analysis of the mechanical improvement induced by lime addition  
590 on a pyroclastic soil. *Eng. Geol.* 221, 193–201.  
591  
592 [8] Scrivener, K.L., Kirkpatrick, R.J., 2008. Innovation in use and research on  
593 cementitious material. *Cem. Concr. Res.* 38, 128–136.  
594  
595 [9] Rahman, A., 1986. The Potentials of Some Stabilizers for the Use of Lateritic Soil in  
596 Construction. *Build. Environ.* 21, 57–61.  
597  
598 [10] Basha, E.A., Hashim, R., Muntohar, A., 2003. Effect of the cement-rice husk ash  
599 on the plasticity and compaction of soil. *Electron. J. Geotech. Eng.* 8.  
600  
601 [11] Nalbantoğlu, Z., 2004. Effectiveness of Class C fly ash as an expansive soil  
602 stabilizer. *Constr. Build. Mater.* 18, 377–381.  
603  
604 [12] Koliass, S., Kasselouri-Rigopoulou, V., Karahalios, A., 2005. Stabilisation of clayey  
605 soils with high calcium fly ash and cement. *Cem. Concr. Compos.* 27, 301–313.  
606  
607 [13] Parsons, R.L., Kneebone, E., 2005. Field performance of fly ash stabilised  
608 subgrades. *Ground Improv.* 9, 33–38.  
609  
610 [14] Sharma, U., Khatri, A., Kanoungoc, A., 2014. Use of Micro-silica as Additive to  
611 Concrete-state of Art. *Int. J. Civ. Eng. Res.* 5, 9–12.  
612  
613 [15] James, J., Pandian, P.K., 2016. Industrial Wastes as Auxiliary Additives to  
614 Cement/Lime Stabilization of Soils. *Adv. Civ. Eng.* 2016, 1–17.  
615  
616 [16] Singhi, B., Laskar, A.I., Ahmed, M.A., 2016. Investigation on Soil–Geopolymer  
617 with Slag, Fly Ash and Their Blending. *Arab. J. Sci. Eng.* 41, 393–400.  
618  
619 [17] Wilkinson, A., Haque, A., Kodikara, J., 2010. Stabilisation of clayey soils with  
620 industrial by-products: part A. *Proc. Inst. Civ. Eng. - Ground Improv.* 163, 149–163.  
621  
622 [18] Cristelo, N., Glendinning, S., Teixeira Pinto, A., 2011. Deep soft soil improvement  
623 by alkaline activation. *Proc. Inst. Civ. Eng. - Ground Improv.* 164, 73–82.  
624  
625 [19] Phummiphan, I., Horpibulsuk, S., Rachan, R., Arulrajah, A., Shen, S-L.,  
626 Chindaprasirt, P. 2018. High Calcium Fly Ash Geopolymer Stabilized Lateritic Soil and  
627 Granulated Blast Furnace Slag Blends as a Pavement Base Material, *Journal of*  
628 *Hazardous Materials*, *Journal of Hazardous Materials*, 341, pp. 257-267  
629 [20] Cristelo, N., Glendinning, S., Fernandes, L., Pinto, A.T., 2012. Effect of calcium  
630 content on soil stabilisation with alkaline activation. *Constr. Build. Mater.* 29, 167–174.  
631

- 632 [21] Rios, S., Cristelo, N., Viana da Fonseca, A., Ferreira, C., 2016. Structural  
633 Performance of Alkali-Activated Soil Ash versus Soil Cement. *J. Mater. Civ. Eng.* 28,  
634 4015125.  
635
- 636 [22] Tenn, N., Allou, F., Petit, C., Absi, J., Rossignol, S., 2015. Formulation of new  
637 materials based on geopolymer binders and different road aggregates. *Ceram. Int.* 41,  
638 5812–5820.  
639
- 640 [23] Sargent, P., Hughes, P.N., Rouainia, M., White, M.L., 2013. The use of alkali  
641 activated waste binders in enhancing the mechanical properties and durability of soft  
642 alluvial soils. *Eng. Geol.* 152, 96–108.  
643
- 644 [24] Zhang, M., Guo, H., El-Korchy, T., Zhang, G., Tao, M., 2013. Experimental  
645 feasibility study of geopolymer as the next-generation soil stabilizer. *Constr. Build.*  
646 *Mater.* 47, 1468–1478.  
647
- 648 [25] Silva, R.A., Oliveira, D.V., Miranda, T., Cristelo, N., Escobar, M.C., Soares, E.,  
649 2013. Rammed earth construction with granitic residual soils: The case study of  
650 northern Portugal. *Constr. Build. Mater.* 47, 181–191.  
651
- 652 [26] Buchwald, A., Kaps, C., Hohmann, M., 2003. Alkali-activated binders and  
653 pozzolan cement binders—complete binder reaction or two sides of the same story, in:  
654 *Proceedings of the 11th International Conference on the Chemistry of Cement.* Portland  
655 *Cement Association Durban, South Africa*, pp. 1238–1246.  
656
- 657 [27] Shi, C., Krivenko, P.V., Roy, D.M., 2006. *Alkali-activated cements and concretes.*  
658 *Taylor & Francis, London ; New York.*  
659
- 660 [28] Sukmak, P., Horpibulsuk, S., Shen, S-L., Chindaprasirt, P., Suksiripattanapong, C.  
661 2013. Factors influencing strength development in clay-fly ash geopolymer, *Constr.*  
662 *Build. Mater.*, 47, 1125-1136.  
663
- 664 [29] Sukmak, P., De Silva, P., Horpibulsuk, S., Chindaprasirt, P. 2015. Sulphate  
665 resistance of clay-Portland cement and clay-high calcium fly ash geopolymer, *J. Mater.*  
666 *Civ. Eng.*, Vol. 27, No. 5, 04014158.
- 667 [30] Snellings, R., Mertens, G., Elsen, J., 2012. *Supplementary Cementitious Materials.*  
668 *Rev. Mineral. Geochem.* 74, 211–278.  
669
- 670 [31] Newman, E.S. 1941. Behaviour of calcium sulfate at high temperatures. *J. of Res.*  
671 *of Nat. Bur. of Stand.*, Vol 27, 191-196.  
672
- 673 [32] Stern, K. H., and Weise, E. L. 1966. High temperature properties and  
674 decomposition of Inorganic salts – Part 1 – Sulfates. *National Standard Reference Data*  
675 *Series- National Bureau of Standards 7, Issued October 1, 52p.*  
676
- 677 [33] Pop S-F., Ion, R.M. 2013. Thermal analysis of the chemical weathering of chalk  
678 stone materials. *J. of Optoelect. And Adv. Mat.*, Vol 15, No. 7- 8, 888 – 892.

- 679 [34] Cong, X., Kirkpatrick, R.J., 1996.  $^{29}\text{Si}$  MAS NMR study of the structure of  
680 calcium silicate hydrate. *Adv. Cem. Based Mater.* 3, 144–156.  
681
- 682 [35] Andersen, M.D., Jakobsen, H.J., Skibsted, J., 2003. Incorporation of Aluminum in  
683 Calcium Silicate Hydrate (C–S–H) of Hydrated Portland Cements: A High-Field  $^{27}\text{Al}$   
684 and  $^{29}\text{Si}$  MAS NMR Investigation. *Inorg. Chem.* 42, 2280–2287.  
685
- 686 [36] Sun, G.K., Young, J.F., Kirkpatrick, R.J., 2006. The role of Al in C–S–H: NMR,  
687 XRD, and compositional results for precipitated samples. *Cem. Concr. Res.* 36, 18–29.  
688
- 689 [37] Pardal, X., Brunet, F., Charpentier, T., Pochard, I., Nonat, A., 2012.  $^{27}\text{Al}$  and  $^{29}\text{Si}$   
690 Solid-State NMR Characterization of Calcium-Aluminosilicate-Hydrate. *Inorg. Chem.*  
691 51, 1827–1836.  
692
- 693 [38] Wilson M.J., 1994. *Clay mineralogy: spectroscopic and chemical determinative*  
694 *methods*, Springer Science + Business Media.  
695
- 696 [39] Knapik K, 2016. Experimental and numerical analyses of fly ash from fluidized  
697 bed combustion applications for selected ground improvement. The Silesian University  
698 of Technology, PhD thesis, 217p.  
699
- 700 [40] Tajuelo Rodriguez, E., Garbev, K., Merz, 650 D., Black, L., Richardson, I.G.,  
701 2017. Thermal stability of C-S-H phases and applicability of Richardson and Groves'  
702 and Richardson C-(A)-S-H(I) models to synthetic C-S-H. *Cem. Concr. Res.* 93, 45–56.  
703
- 704 [41] Provis John L., van Deventer Jannie S.J., 2009. *Geopolymers Structure,*  
705 *processing, properties and industrial applications*, Woodhead Publishing in materials.  
706 Woodhead, Cambridge.  
707
- 708 [42] Occhipinti R., Tarantino S. C., Riccardi M. P., Sturini M., Speltini A., Maraschi F.,  
709 Elmaleh A., Zema M., 2017. Alkali activation of sulfate-bearing kaolin. *Proceedings of*  
710 *the 16th International Clay Conference*, Granada, Spain.  
711